Acta Crystallographica Section D
Biological Crystallography
ISSN 0907-4449

Structure of creatine amidinohydrolase from *Actinobacillus*

Balasundaram Padmanabhan,[a] Arno Paehler[b] and Masami Horikoshi[a,c]*

[a]Horikoshi Gene Selector Project, Exploratory Research for Advanced Technology (ERATO), Japan Science and Technology Corporation (JST), 5-9-6 Tokodai, Tsukuba, Ibaraki 300-2635, Japan, [b]RIKEN Harima Institute, High Throughput Factory, Protein Structural Information Team, 1-1-1 Kouto, Mikazuki-cho, Hyogo 679-5148, Japan, and [c]Laboratory of Developmental Biology, Institute of Molecular and Cellular Biosciences, The University of Tokyo, 1-1-1 Yayoi, Bunkyo-ku, Tokyo 110-0032, Japan

Correspondence e-mail: horikosh@iam.u-tokyo.ac.jp

Received 12 March 2002
Accepted 6 June 2002

PDB Reference: creatinase, 1kp0, r1kp0sf.

The crystal structure of *Actinobacillus* creatine amidinohydrolase has been solved by molecular replacement. The amino-acid sequence has been derived from the crystal structure. Crystals belong to space group *I*222, with unit-cell parameters $a = 111.26$ (3), $b = 113.62$ (4), $c = 191.65$ (2) Å, and contain two molecules in an asymmetric unit. The structure was refined to an *R* factor of 18.8% at 2.7 Å resolution. The crystal structure contains a dimer of 402 residues and 118 water molecules. The protein structure is bilobal, consisting of a small N-terminal domain and a large C-terminal domain. The C-terminal domain has a pitta-bread fold, similar to that found in *Pseudomonas putida* creatinase, proline aminopeptidases and methionine aminopeptidase. Comparison with complex crystal structures of *P. putida* creatinase reveals that the enzyme activity of *Actinobacillus* creatinase might be similar to that of *P. putida* creatinase.

1. Introduction

Creatininase (EC 3.5.2.10; creatinine amidohydrolase) is the first enzyme in the metabolic degradation pathway of creatinine that hydrolyses creatinine to creatine. Subsequently, creatine is transformed into sarcosine and urea in a second hydrolyzation step by creatinase (EC 3.5.3.3; creatine amidinohydrolase). Sarcosine is demethylated by sarcosine oxidase (EC 1.5.3.1) (Roche *et al.*, 1950) or sarcosine dehydrogenase (EC 1.5.99.1) to produce glycine and formaldehyde (Tsuru *et al.*, 1976). Creatine is generally found in the blood, brain and muscle of many living organisms. Creatinine occurs in these cells as the only intermediate product of creatine metabolism. Measurement of the creatinine levels in serum and determination of the renal clearance of creatinine are widely used for laboratory diagnosis of renal and muscular function (Madaras & Buck, 1996). Both compounds, creatinine and creatine, can be used by microorganisms as carbon and nitrogen sources (Tsuru, 1977). Creatinase is also found in microorganisms, such as *Pseudomonas putida* DSM2106 (Hoeffken *et al.*, 1988), *Flavobacterium* sp. U-188 (Koyama *et al.*, 1990) and *Bacillus* sp. B-0618 (Suzuki *et al.*, 1993), and plays a general role in microbial creatinine degradation.

Other than creatinases, many other amidinohydrolases are found; namely, proline aminopeptidases (AMPPs; Wilce *et al.*, 1998) and methionine aminopeptidases (AMPMs; Roderick & Matthews, 1993; Tahirov *et al.*, 1998; Liu *et al.*, 1998). Structural comparisons between creatinase and AMPM and AMPP hydrolases and sequence comparisons between these proteins have suggested that the catalytic domain of all these enzymes shares a common pitta-bread fold (Bazan *et al.*, 1998).

The crystal structure analysis and enzymatic mechanism of creatinase from *P. putida* have been reported (Hoeffken *et al.*, 1988; Coll *et al.*, 1990). This is the only creatinase protein structure available to date in the Protein Data Bank. *Actinobacilli* are Gram-negative rod-shaped aerobic and parasitic bacteria. They are pathogenic for animals and hence are clinically important because of their resistance to most antibiotics. Since creatinine and creatine can be used by microorganisms as carbon and nitrogen sources, creatinase may play a role in the disease process caused by *Actinobacillus*. Therefore, we have initiated crystallographic studies of creatinase from *Actinobacillus* in order to understand its functional role in *Actinobacillus* and also for structural relationship studies of creatinases at the tertiary structure level.

Here, we report the structure of *Actinobacillus* creatinase (hereafter referred to as *Ac.* creatinase) at 2.7 Å resolution, compare it with that of creatinase from *P. putida* (hereafter, *Pp*. creatinase) and extrapolate the enzyme activity of *Ac.* creatinase based on sequence conservation and complex crystal structures of *Pp*. creatinase. Since the amino-acid sequence of *Ac.* creatinase is at present not available in databases, its sequence has been derived from the crystal structure.

Table 1
Data-collection and refinement statistics.

Space group	*I*222
Unit-cell parameters (Å)	a = 111.26 (3), b = 113.62 (4), c = 191.65 (2)
Resolution range (Å)	30.0–2.7
No. of measured reflections	167670
No. of unique reflections	33902
$R_{\rm merge}$† (%)	6.5 (15.1)‡
Completeness (%)	99.8 (99.9)‡
Average $I/\sigma(I)$	10.6 (4.9)‡
R factor§ (%)	18.8
$R_{\rm free}$¶	22.2
B values (Å^2)	
Main chain (chain A)	18.01
Main chain (chain B)	17.93
Side chains (chain A)	19.43
Side chains (chain B)	19.45
Waters	19.13
R.m.s. deviations	
Bond lengths (Å)	0.007
Bond angles (°)	1.32
No. of residues in the protein	402
No. of chains in the asymmetric unit	2
No. of water molecules	118

† $R_{\rm merge} = \sum |I(h) - \langle I(h)\rangle| / \sum I(h)$, where $I(h)$ is the observed intensity and $\langle I(h)\rangle$ is the mean intensity of reflection h over all measurements of $I(h)$. ‡ Values in parentheses are for the last shell, 2.85–2.70 Å. § R factor $= \sum(F_{\rm obs} - kF_{\rm calc}) / \sum_{hkl} F_{\rm obs}$, where k is a scale factor. ¶ $R_{\rm free}$ is the R factor for the test set of reflections not used during refinement (5% of the data set).

2. Materials and methods

2.1. Crystallization and data collection

Ac. creatinase was purchased from Toyobashi Ltd (Japan). Crystals obtained by the hanging-drop vapour-diffusion method were subsequently microseeded, followed by macroseeding as described previously (Padmanabhan & Horikoshi, 2002). Briefly, tiny crystals were initially obtained with 15–20% PEG 6K, 0.1 *M* sodium citrate pH 5.0. These crystals were crushed into microcrystals and then used for microseeding. Many crystals in the microseeded drops were grown with defects that could be visualized through a microscope and did not grow to a size sufficient for X-ray diffraction. Hence, the non-defective crystals were selected by checking through a microscope before macroseeding. Crystals of dimensions of approximately 0.25 × 0.2 × 0.06 mm were obtained in a drop containing 2 µl 10.0 mg ml^{-1} protein solution and 2 µl reservoir solution containing 10% PEG 6K, 0.1 *M* sodium citrate pH 5.0.

The data collection was carried out with a single crystal on beamline BL18B of the Photon Factory, Tsukuba, Japan using an ADSC Quantum-4 CCD detector. A complete data set was obtained at room temperature to a maximum resolution of 2.7 Å. All data were processed and scaled using the programs *DPS*/*MOSFLM* (Rossmann & van Beek, 1999) and *SCALA* from the *CCP*4 package (Collaborative Computational Project, Number 4, 1994). The unit-cell parameters of these crystals are a = 111.26, b = 113.62, c = 191.65 Å and they belong to the orthorhombic *I*222 crystal system. The processed data are 99.8% complete to 2.7 Å resolution.

2.2. Structure determination and refinement

A self-rotation function indicated that two molecules are related by non-crystallographic twofold symmetry. Solvent content, calculated by the Matthews method (Matthews, 1968), is 62% for two molecules per asymmetric unit. The *Ac.* creatinase structure was solved by molecular replacement with *AMoRe* (Navaza, 1994) using normalized structure-factor amplitudes and with the *Pp*. creatinase protein structure as the search model. Molecular-replacement calculations were carried out with diffraction data in the resolution range 15–4.0 Å. Initially, a monomer was used as a search model. Since the monomer model did not give a correct solution for the translation function, a dimer was then used as the search model to calculate rotation and translation functions. Peaks in the cross-rotation function used for the two-body translation-function (TF) search with a subsequent rigid-body refinement gave a high contrast peak with a correlation coefficient of 0.407 and an R factor of 47.3%.

The correctly oriented molecule's side chains were truncated to Ala for all residues before initiating rigid-body refinement. After rigid-body refinement, the structure was subjected to molecular-dynamics simulated annealing from 3000 K to reduce model phase bias using the program *CNS* (Brünger *et al.*, 1998). A test data set containing 5% of reflections from the data set was selected to examine the $R_{\rm free}$ throughout the entire refinement process. Based on $(2F_o - F_c)$ and $(F_o - F_c)$ electron-density maps, the structure was rebuilt with the graphics program *O* (Jones *et al.*, 1991). The initial R factor and $R_{\rm free}$ were 39.0 and 40.2%, respectively, and the $(2F_o - F_c)$ map generated by *CNS* calculated after the first

cycle of refinement showed that the model fitted the electron density well and was readily interpretable for many side chains. The main chain of all residues and their side chains could be unambiguously identified by their electron density. In order to clarify the identity of some side chains, *e.g.* Asp and Asn, Gln and Glu, Thr and Val, His and Phe, the local environment around the residues, especially their ability to form hydrogen bonds and/or salt bridges with neighbouring groups, was taken into account, together with the sequence of *Pp*. and *Bacillus* creatinases, during identification of the side chains. The side chains were fitted into their corresponding electron density whenever they were clearly visible, with simultaneous careful monitoring of the main-chain tracing. Several rounds of simulated annealing with grouped temperature factors were performed until all possible side chains were identified. A series of omit maps was used to inspect and confirm the amino-acid assignments. 118 water molecules were included at the final stage of refinement. For any unknown protein sequence, the correct sequence can be determined from its tertiary structure solved at atomic resolution. Since the reflection data was only to 2.7 Å resolution, which was not sufficient to identify ambiguous residues (especially Gln/Glu and Asn/Asp) correctly, the following steps were taken into account at the end of the final refinement. Residues (Asp, Asn, Glu and Gln) which are conserved between *Pp*. and *Bacillus* were treated as the same corresponding residues at equivalent positions in *Ac*. creatinase or otherwise treated as Asx or Glx. The positions of ambiguous residues, labelled Asx and Glx, which were determined from the above analyses are as follows. Glx: 5, 7, 13, 21, 28, 68, 72, 119, 134, 136, 149, 154, 163, 168, 204, 240, 267, 268, 275, 278, 289, 310 and 345. Asx: 29, 39, 71, 94, 130, 164, 199, 208, 236, 270, 306, 329, 362 and 384. Tight NCS restraints for the dimer in the asymmetric unit were used throughout the refinement. The stereochemistry of the refined structure was analyzed with the program *PROCHECK* (Laskowski *et al.*, 1993). The program *LSQKAB* from *CCP*4 was used to calculate r.m.s. deviations for the superposition of molecules.

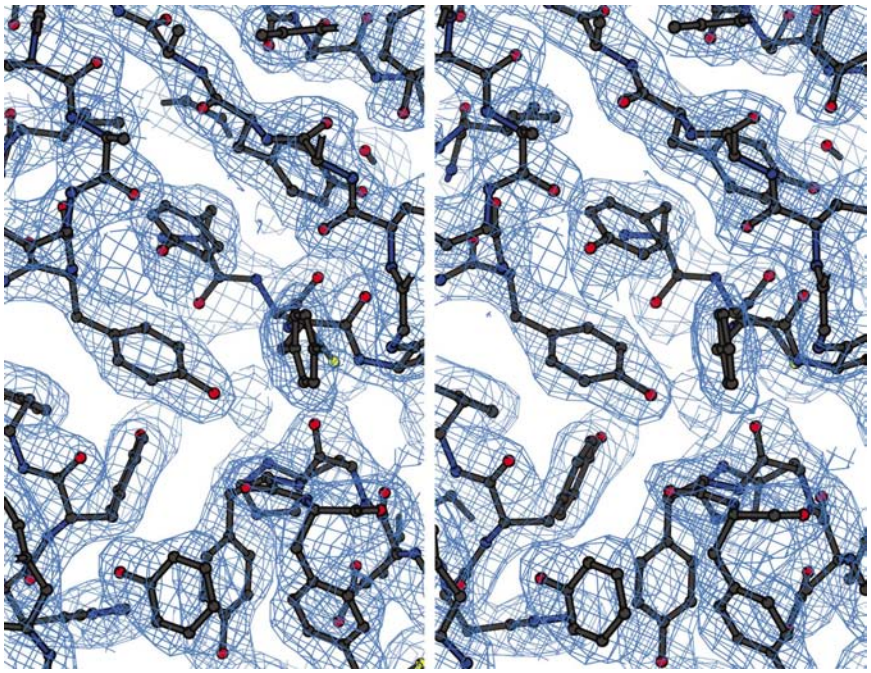

Figure 1
Stereoview of the refined ($2F_o - F_c$) electron-density map at 2.7 Å resolution. The map is contoured at 1σ, with the final model displayed for comparison. The figure was prepared using the program *BOBSCRIPT* (Kraulis, 1991; Esnouf, 1997).

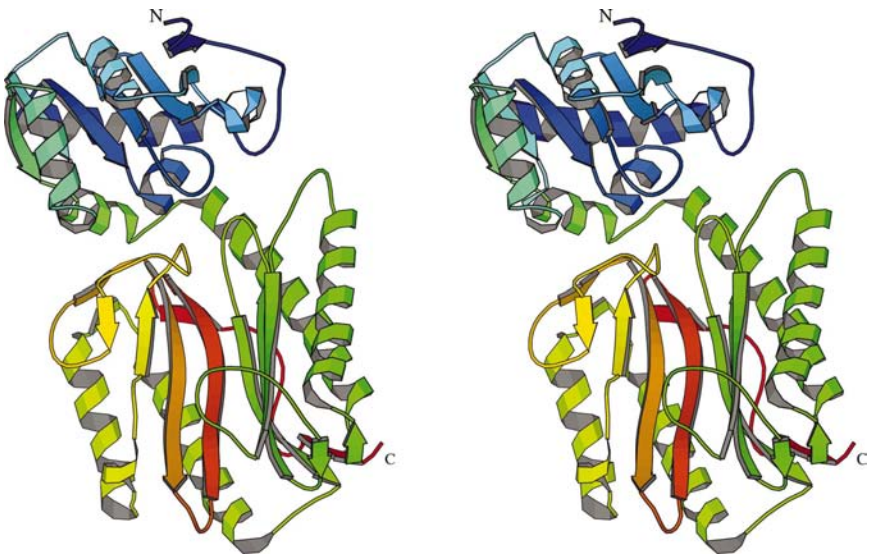

Figure 2
Stereoview of ribbon diagram of *Ac*. creatinase showing two domains in the protein. The figure was drawn using *MOLSCRIPT* (Kraulis, 1991).

2.3. Thermal vibration parameters

The average *B* factors for main-chain atoms in chain *A* and in chain *B* are 18.01 and 17.93 Å^2, respectively, while those for side-chain atoms in chain *A* and chain *B* are 19.43 and 19.45 Å^2, respectively. *B* factors for water molecules range from 5.0 to 34.45 Å^2, with an average of 19.13 Å^2 (Table 1).

3. Results and discussion

3.1. Quality of the model

The crystal structure of *Ac*. creatinase was determined by molecular replacement using the *Pp*. creatinase structure as the search model. The asymmetric unit contains two

molecules, which are related by twofold NCS symmetry. Final refinement of the structure resulted in an R factor of 18.8% and an $R_{\rm free}$ of 22.2%. The final electron-density map (Fig. 1) for the refined model contains continuous electron density for residues 2–402 of the polypeptide chain. The Ramachandran map suggests that the overall rating for the model is 'good'. *PROCHECK* (Laskowski *et al.*, 1993) analysis showed that 90% of residues are located in the most favoured region of the Ramachandran diagram. Two residues (Glx267, Arg334) from each monomer are in the disallowed regions of high conformational energy. Glx267 lies in a tight turn which connects strand β12 with helix α9 and analysis of the $(2F_o - F_c)$ electron-density map ascertains their conformation. The protein contains 31 glycine residues and 15 proline residues. The G factor, a global measure for the quality of protein stereochemistry, is 0.28.

3.2. Overall description

Ac. creatinase is a homodimer with a monomer size of 402 amino acids. The *Ac*. creatinase tertiary structure can be divided into two well defined domains similar to the domains of *Pp*. creatinase (Coll *et al.*, 1990). The small N-terminal domain contains 160 residues and the larger C-terminal domain 240 residues. The overall topology of *Ac*. creatinase is shown in Fig. 2.

The N-terminal domain consists of a central seven-stranded β-pleated sheet (β1–β7) flattened by six α-helices (α1–α6). The strands are a mixture of parallel and antiparallel strands; four of the helices (α1–α3 and α6) are attached to the side of the sheet that faces the other domain. The surface side of the sheet, facing the solvent, is connected by the two α-helices α4 and α5.

The secondary-structure elements of the C-terminal domain consist of a sheet of five long strands (β9, β11, β12, β17 and β18), five helices (α7–α11) and two extended loops (residues 225–236 and 325–337). All of the helices except α11 run nearly parallel to the β-sheet. As seen in Fig. 2, these structural elements are related by approximate twofold symmetry. A trough is formed by strands β18 and β12, which are connected by two main-chain hydrogen bonds (Glu261 O–His375 N, Thr263 N–Arg373 O). The putative active site is located in the centre of this trough (Fig. 2). The trough is stabilized by four helices (α7–α10) that cover the exterior of the trough. The C-terminal segment containing β-strands β19 and β20 is located at the bottom of the trough between helices α7 and α9.

A small segment, residues 156–158, connects the N- and C-terminal domains. There are few non-bonded interactions between these two domains and six electrostatic interactions between them. Of these six, two are main-chain–side-chain interactions (Ser20 N–Glu161 OE1 and Asn52 ND2–Phe254 O), while the other four are side-chain–side-chain interactions (Ser20 OG–Glu161 OE2, Arg26 NH2–Glu162 OE1, Arg90 NE–Glu213 OE1 and Arg90 NE–Glu213 OE2). The residues involved in electrostatic interactions between the lobes found in *Pp*. creatinase differ from those found in *Ac*. creatinase, except for the Ser20 N–Glu161 OE1 (Glu162 in *Pp*. creatinase) interaction.

Table 2
Hydrogen-bonding interactions between *Ac*. creatinase and its symmetry-related molecules.

Protein atom	Symmetry-related protein atom	Distance (Å)
Asx*A*29 O	Glu*A*349 OE2	2.69
Asx*A* 39O	Glx*A*345 OE2/NE2	3.16
Glx*A*72 NE2/OE2	Arg*A*296 NH1	2.78
Lys*A*137 NZ	Lys*A*118 NZ	3.44
Lys*A*137 NZ	Gly*B*116 O	3.46
Arg*A*207 NH1	Arg*A*207 O	2.92
Arg*A*207 O	Arg*A*207 NH1	2.92
Glx*A*240 NE2/OE2	Asx*B*306 OD2/ND2	3.32
Lys*B*14 O	Lys*B*279 NZ	3.29
Lys*B*37 O	Trp*B*153 NE1	2.88
Asx*B*39 OD2/ND2	Arg*A*133 NH2	3.37
Lys*B*118 NZ	Lys*A*137 NZ	3.44
Gly*B*116 O	Lys*A*137 NZ	3.46

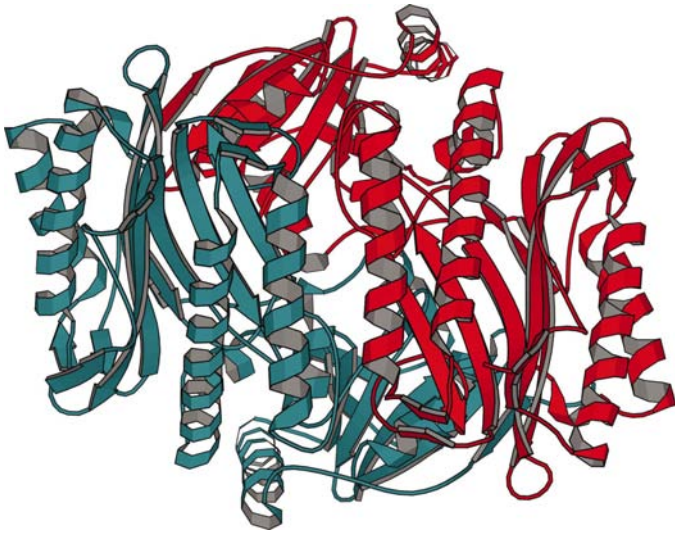

Figure 3
Ribbon diagram of dimeric arrangement of *Ac*. creatinase. The figure was prepared using the program *MOLSCRIPT* (Kraulis, 1991).

3.3. Crystal packing

Salt bridges or hydrogen bonds formed directly between symmetry-related *Ac*. creatinase molecules are listed in Table 2. *Ac*. creatinase has a total of 12 symmetry-related intermolecular interactions. Eight of the crystal contacts are main-chain–side-chain interactions, two are side-chain–side-chain interactions and three are salt bridges. *Ac*. creatinase crystallizes in *I*222 symmetry, whereas *Pp*. creatinase crystallizes in $P2_1$. Intermolecular contacts were calculated with the program *ACT* (Collaborative Computational Project, Number 4, 1994). The cutoff used for intermolecular contacts was 3.5 Å maximum, but the exact value depended on atom type and standard van der Waals radii.

Table 3
Hydrogen-bonding interactions between the *A* and *B* chains of the dimers.

Protein atom	Protein atom	Distance (Å)
Main chain–main chain		
Phe*A*62 N	His*B*330 O	2.85
Ile*A*82 N	Thr*B*318 O	3.40
Ile*A*82 O	Ala*B*230 N	2.87
His*A*124 O	Leu*B*129 N	3.06
His*A*124 O	Asx*B*130 N	2.82
Val*A*127 O	Leu*B*129 N	3.05
Leu*A*129 N	His*B*124 O	3.12
Leu*A*129 N	Val*B*127 O	3.08
Asx*A*130 N	HisB124 O	2.92
Leu*A*214 N	Val*B*234 O	2.82
Ala*A*230 N	Ile*B*82 O	2.94
Val*A*234 O	Leu*B*214 N	2.80
Thr*A*318 O	Ile*B*82 N	3.19
His*A*330 O	Phe*B*62 N	2.94
Main chain–side chain		
Phe*A*62 O	Arg*B*334 NH1	2.84
Gly*A*85 N	Asp*B*228 OD2	2.81
Arg*A*103 N	Asp*B*343 OD2	3.22
Val*A*212 N	Asp*B*236 OD1	3.43
Gly*A*320 N	Asp*B*100 OD2	3.13
Glu*A*364 N	Asn*B*11 OD1	2.77
Gly*B*85 N	Asp*A*228 OD2	2.79
Arg*B*103 N	Asp*A*343 OD2	2.96
Val*B*212 N	Asx*A*236 OD1/ND1	3.35
Thr*B*318 O	Lys*A*80 NZ	3.45
Gly*B*320 N	Asp*A*100 OD2	3.16
Asp*B*343 O	Arg*A*103 NH2	3.13
Side chain–side chain		
Arg*A*89 NH1	Asp*B*228 OD2	2.49
Arg*A*89 NH2	Asp*B*228 OD1	3.05
Arg*A*103 NE	Asp*B*343 OD2	2.91
Glu*A*192 OE1	Arg*B*203 NH1	2.89
Glu*A*192 OE2	Arg*B*203 NH1	2.62
Arg*A*203 NH1	Glu*B*192 OE1	2.54
Arg*A*203 NH1	Glu*B*192 OE2	2.86
Asp*A*228 OD1	Arg*B*89 NH2	3.18
Asp*A*228 OD1	Arg*B*89 NH1	3.20
Asp*A*228 OD2	Arg*B*89 NH1	2.66
Asp*A*228 OD2	Asn*B*11 ND2	3.08

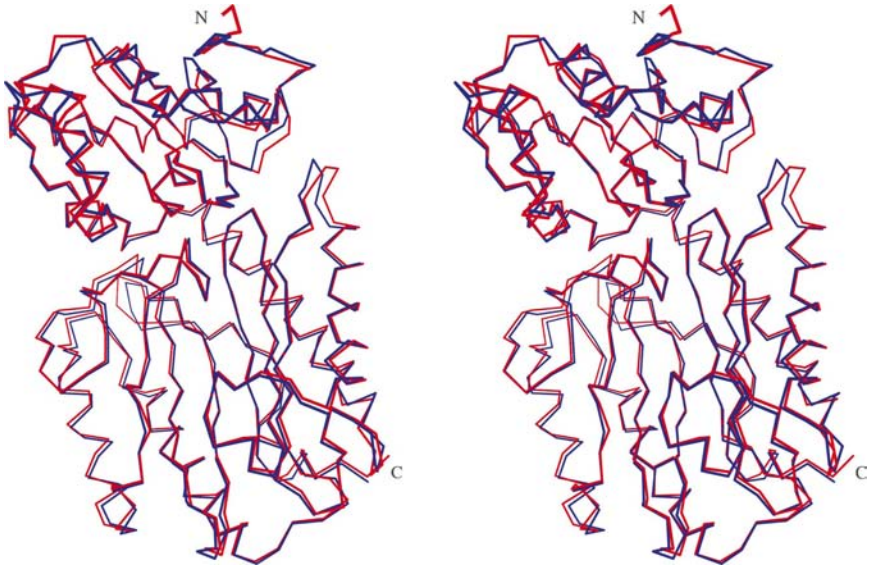

Figure 4
Stereoview of the superposed C^{α} traces of the *Ac.* (red) and *Pp.* (blue) creatinase structures. The figure was drawn using *MOLSCRIPT* (Kraulis, 1991).

3.4. Dimer interactions

The ribbon diagram of the *Ac.* creatinase dimer is shown in Fig. 3. A single monomer of *Ac.* creatinase has an accessible surface area of 17 020 Å^2. When forming a homodimer, the accessible surface is drastically reduced to 13 455 Å^2. The electrostatic interactions formed between the two monomers are listed in Table 3. The dimer is stabilized by 14 main-chain hydrogen bonds formed by Phe62 N–His330 O, Ile82 N–Thr318 O, Ile82 O–Ala230 N, His124 O–Leu129 N, His124 O–Asx130 N, Val127 O–Leu129 N, Leu214 N–Val234 O and symmetrically equivalent pairs. Salt bridges are formed by Arg89–Asp228, Arg103–Asp343, Glu192–Arg203 and symmetrically equivalent pairs. The secondary-structural elements involved in dimerization include the loop between α2 and β3, helix α3, the loop between β5 and α4, the turn between β6 and α5, helix α8, the loop between α8 and α9, the extended loop between β9 and β10, the turn between α11 and β14 and the extended loop between β14 and β15.

3.5. Comparison studies

Since the refinement had been carried out with tight NCS restraints between the monomers, superposition of main-chain atoms of chain *A* with those of chain *B* results in an r.m.s. deviation of 0.23 Å. Therefore, most of the subsequent discussion is based on the coordinates of one monomer of the asymmetric unit dimer.

Superposing C^{α} atoms of the *Ac.* creatinase monomer (6–86, 95–159, 160–399) with the equivalent atoms of a *Pp.* creatinase monomer (6–86, 96–160, 161–400) gives an r.m.s. deviation of 0.62 Å (Fig. 4). The maximum r.m.s. deviation of 2.73 Å was observed at Thr18, which is replaced by Pro18 in *Ac.* creatinase. The X-ray structure studies show that the overall folds of *Ac.* creatinase and *Pp.* creatinase are quite similar. Larger sequence variations (Fig. 5) were found in the N-terminal domain than in the C-terminal domain. In the C-terminal domain, sequence variations are located mainly in the secondary-structure elements α7, α8, α9, α10 and β10. As the sequence of *Ac.* creatinase was derived from its tertiary structure using *Pp.* creatinase as a starting model, we predict that the tertiary structure of *Bacillus* creatinase will also be similar to these two known creatinase tertiary structures.

The present work provides additional structural data on the striking similarities between creatinases, proline aminopeptidases (AMPPs; Wilce *et al.*, 1998) and methionine aminopeptidases (AMPMs; Roderick & Matthews, 1993; Tahirov *et al.*, 1998; Liu *et al.*, 1998). The catalytic C-terminal domains of these three protein classes all have the same pitta-bread fold (Bazan *et al.*, 1994). Although the C-terminal domains of these proteins have a similar fold, the enzyme mechanism of

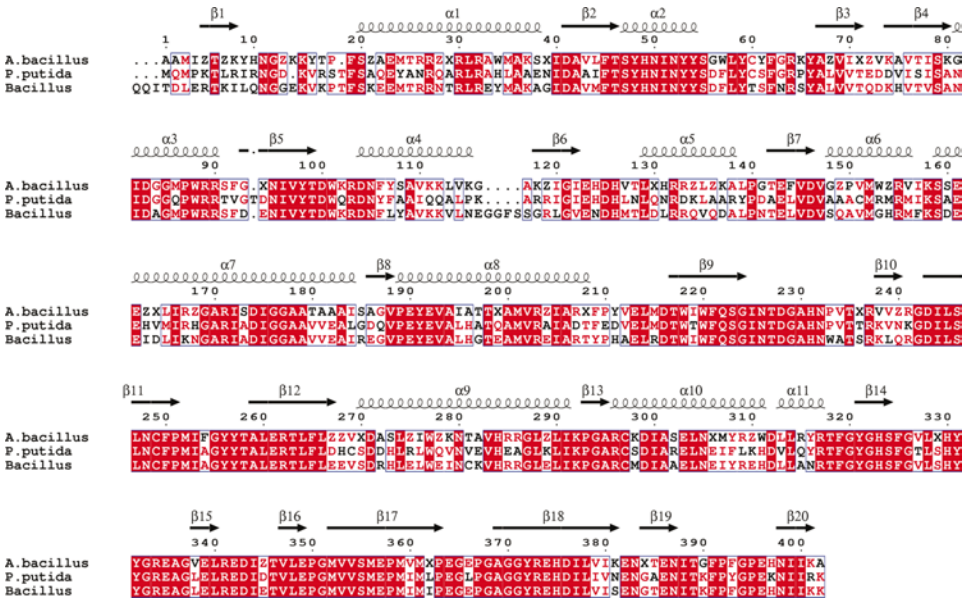

Figure 5
Sequence alignment of *Ac.* creatinase with other homologous proteins. Secondary structures of *Ac.* creatinase are shown by arrows and helices. The alignment was produced by *CLUSTALW* (Higgins *et al.*, 1992). Sequences used in this figure were obtained from the Entrez database: P38488 (*P. putida*) and P38487 (*Bacillus*). The ambiguous residues Asx (Asp/Asn) and Glx (Glu/Gln) are denoted by X and Z, respectively. The figure was produced using *ESPRIPT* (Gouet *et al.*, 1999).

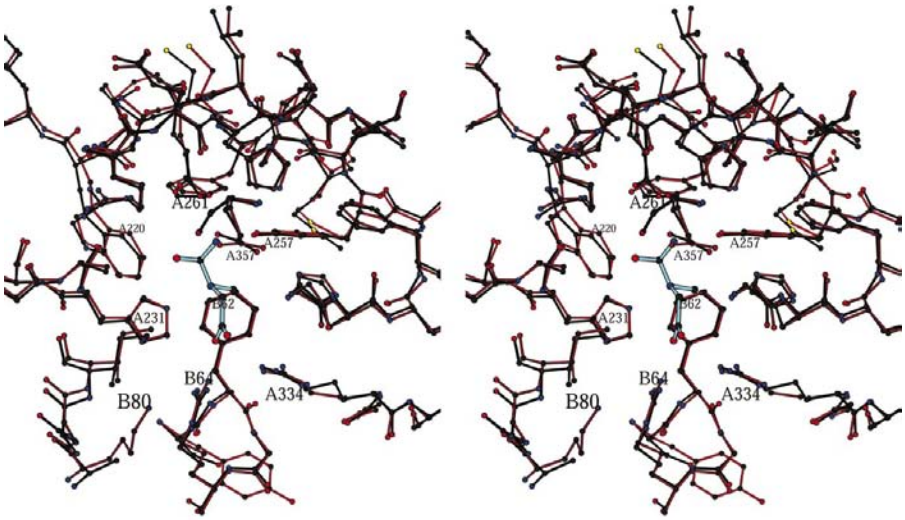

Figure 6
Superimposed binding sites of the *Ac.* creatinase (red) and the *Pp.* creatinase (black)–carbamyol sarcosine (cyan) complex. The figure was produced using *MOLSCRIPT* (Kraulis, 1991).

creatinases (Coll *et al.*, 1990) is distinct from that of AMPP and AMPM. The creatinase protein is not metal dependent, whereas AMPP and AMPM are metal-dependent enzymes (Mn^{2+} in AMPP; Co^{2+} centre in AMPM). Surprisingly, the N-terminal domains of creatinase and AMPP also have similar folds. Although the overall tertiary structure of creatinase here is similar to that of AMPP, the sequence identity between them is substantially lower. When the sequence alignments of *Ac.* creatinase, *Pp.* creatinase, AMPP, AMPM and prolidases were compared, we found only 13 conserved residues (data not shown). Despite the fact that the overall tertiary structures of creatinase and AMPP are similar, the oligomerization of creatinase (dimer) differs from the AMPP oligomerization (tetramer) (Wilce *et al.*, 1998).

3.6. Active site

The active site is deeply buried and located in an oval-shaped depression in the inner surface of the trough which is formed by the larger domain. The ends of the depression are defined by two loops (residues 225–236 and residues 325–337). The substrate-binding pocket is covered by the N-terminal small domain of the other subunit (Fig. 3). Complex crystal structures of *Pp.* creatinase with carbamoyl sarcosine, creatine, succinamic acid and HCO_3^- have been reported (Coll *et al.*, 1990) and a putative enzyme mechanism for *Pp.* creatinase has been derived on the basis of these complex crystal structures (Coll *et al.*, 1990).

The carbamoyl sarcosine model was placed in the *Ac.* creatinase active site in approximately the same orientation as the carbamoyl sarcosine in the *Pp.* creatinase complex structure (Fig. 6). The active-site residues in *Pp.* creatinase are Phe62, Arg64, His232, Tyr258, Glu262, Arg335, Glu358 and His376. These residues are highly conserved with their counterparts in *Ac.* creatinase. The corresponding conserved residues in *Ac.* creatinase are Phe62, Arg64, His231, Tyr257, Glu261, Arg334, Glu357 and His375, respectively. No major differences are observed in the position of the residues forming the active site, providing evidence for the rigidity of this region of the protein. A total of ten hydrogen bonds were observed between *Ac.* creatinase and the carbamoyl sarcosine model. The residues involved in the catalysis in *Pp.* creatinase are highly conserved with equivalent *Ac.* creatinase residues. Near the binding pocket in *Ac.* creatinase, residue Lys80, which is replaced by Ala80 in *Pp.* creatinase, might be involved in catalysis. The molecule forms three strong interactions with creatine: the guanidinium group of creatine binds to Glu*A*261 and Glu*A*357, the carboxylate group to Arg*B*64

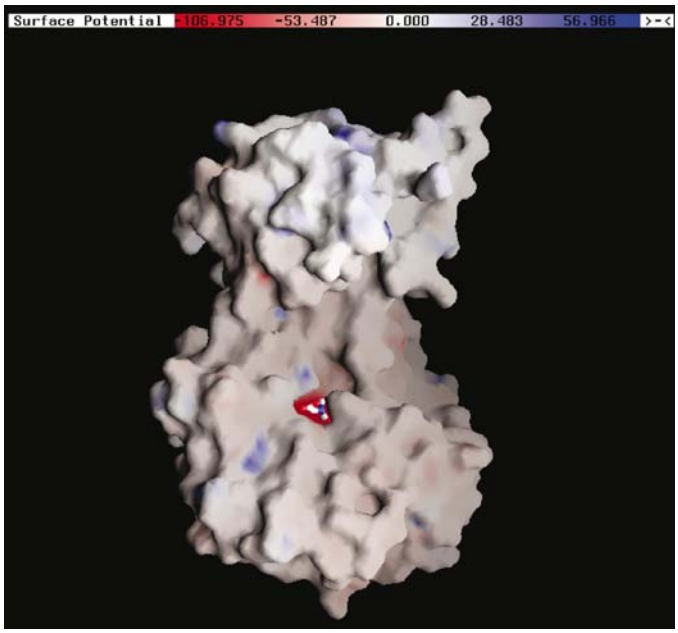

Figure 7
Electrostatic potential surface of the *Ac*. creatinase with modelled substrate. Red represents negative potential, blue represents positive potential and white is neutral. The figure was prepared using *GRASP* (Nicholls *et al.*, 1991).

and Arg*A*334 and there is a van der Waals contact between the methyl group and Phe*B*62. Finally, His*A*231 NE2 is close to all three substructures of creatine. These interactions and the conformation of the substrate are the basis of the catalytic mechanism of creatinase.

The electrostatic potential surface of the model complex with carbamoyl sarcosine was calculated with *GRASP* (Nicholls *et al.*, 1991). The N-terminal domain is rather more hydrophobic than the C-terminal domain. The active site is negatively charged, as shown in Fig. 7. Since the orientation of conserved catalytic residues in *Ac*. creatinase is similar to that in *Pp*. creatinase, we infer that the enzyme mechanism of *Ac*. creatinase might also be very similar to that of *Pp*. creatinase.

This work is supported in part by Grants-in-Aid for Science Research from the Ministry of Education, Science, Sports and Culture of Japan, New Energy and Industrial Technology Development Organization (NEDO) and the Exploratory Research for Advanced Technology (ERATO) of the Japan Science and Technology Corporation (JST).

References

Bazan, J. F., Weaver, L. H., Roderick, S. L., Huber, R. & Matthews, B. W. (1994). *Proc. Natl Acad. Sci. USA*, **91**, 2473–2477.
Brünger, A. T., Adams, P. D., Clore, G. M., DeLano, W. L., Gros, P., Grosse-Kunstleve, R. W., Jiang, J. S., Kuszewski, J., Nilges, M., Pannu, N. S., Read, L. M., Simonson, T. & Warren, G. L. (1998). *Acta Cryst.* D**54**, 905–921.
Coll, M., Knof, S. H., Ohga, Y., Messerschmidt, A., Huber, R., Moellering, H., Russmann, L. & Schumacher, G. (1990). *J. Mol. Biol.* **214**, 597–610.
Collaborative Computational Project, Number 4 (1994). *Acta Cryst.* D**50**, 760–763.
Esnouf, R. M. (1997). *J. Mol. Graph.* **15**, 505–524.
Gouet, P., Courcelle, E., Stuart, D. & Metoz, F. (1999). *Bioinformatics*, **15**, 305–308.
Higgins, D. G., Bleasby, A. J. & Fuchs, R. (1992). *Comput. Appl. Biosci.* **8**, 189–191.
Hoeffken, H. W., Knof, S. H., Bartlett, P. A., Huber, R., Moellering, H. & Schumacher, G. (1988). *J. Mol. Biol.* **204**, 417–433.
Jones, T., Zou, J.-Y., Cowan, S. W. & Kjeldgaard, M. (1991). *Acta Cryst.* A**47**, 110–119.
Koyama, Y., Kitao, S., Yamamoto-Otake, H., Suzuki, M. & Nakano, E. (1990). *Agric. Biol. Chem.* **54**, 1453–1457.
Kraulis, P. J. (1991). *J. Appl. Cryst.* **24**, 946–950.
Laskowski, R. A., MacArthur, M. W., Moss, D. S. & Thornton, J. M. (1993). *J. Appl. Cryst.* **26**, 283–291.
Liu, S., Widom, J., Kemp, C. W., Crews, C. M. & Clardy, J. (1998). *Science*, **282**, 1324–1327.
Madaras, M. B. & Buck, R. P. (1996). *Anal. Chem.* **68**, 3832–3839.
Matthews, B. W. (1968). *J. Mol. Biol.* **33**, 491–497.
Navaza, J. (1994). *Acta Cryst.* A**50**, 157–163.
Nicholls, A., Sharp, K. & Honig, B. (1991). *Proteins Struct. Funct. Genet.* **11**, 281.
Padmanabhan, B. & Horikoshi, M. (2002). *Acta Cryst.* D**58**, 322–323.
Roche, J., Lacombe, G. & Girard, H. (1950). *Biochim. Biophys. Acta*, **6**, 210–216.
Roderick, S. L. & Matthews, B. W. (1993). *Biochemistry*, **32**, 3907–3912.
Rossmann, M. G. & van Beek, C. G. (1999). *Acta Cryst.* D**55**, 1631–1653.
Suzuki, K., Sagai, H., Imamura, S. & Sugiyama, M. (1993). *J. Ferment. Bioeng.* **76**, 77–81.
Tahirov, T. H., Oki, H., Tsuhihara, T., Ogasahara, K., Yutani, K., Ogata, K., Izu, Y., Tsunasawa, S. & Kato, I. (1998). *J. Mol. Biol.* **284**, 101–124.
Tsuru, D. (1977). *Nucleic Acids Amino Acids*, **35**, 31–37.
Tsuru, D., Oka, I. & Yoshimoto, T. (1976). *Agric. Biol. Chem.* **40**, 1011–1018.
Wilce, M. C. J., Bond, C. S., Dixon, N. E., Freeman, H. C., Guss, J. M., Lilley, P. E. & Wilce, J. A. (1998). *Proc. Natl Acad. Sci. USA*, **95**, 3472–3477.